Monte Carlo simulations of two-dimensional fermion systems with string-bond states

J.-P. Song and R. T. Clay*

Department of Physics and Astronomy and HPC^2 Center for Computational Sciences, Mississippi State University, Mississippi State, Mississippi 39762, USA

(Received 17 May 2013; revised manuscript received 15 January 2014; published 3 February 2014)

We describe an application of variational Monte Carlo to two-dimensional fermionic systems within the recently developed tensor-network string-bond state ansatz. We use a combination of variational Monte Carlo and stochastic optimization to optimize the matrix-product state matrices representing the ground state. We present results for a two-dimensional spinless fermion model including nearest-neighbor Coulomb interactions and determine using finite-size scaling the phase boundary between charge-ordered insulating and metallic phases. This approach can treat frustrated systems and be easily extended to fermion models with spin.

DOI: 10.1103/PhysRevB.89.075101 PACS number(s): 02.70.Ss, 71.10.Fd, 71.10.Hf

I. INTRODUCTION

The properties of two-dimensional (2D) and frustrated quantum many-body models play an important role in condensed matter physics. Numerical methods including quantum Monte Carlo (QMC) [1] and the density matrix renormalization group (DMRG) [2–4] have been essential in understanding the ground-state and thermodynamic properties of interacting electron and spin systems. These two classes of methods have well-known limitations, however, the fermion sign problem severely limits the systems that can be studied by QMC, and DMRG methods are largely limited to one-dimensional (1D) or quasi-1D systems.

Underlying DMRG methods is a matrix product state (MPS) representation of the quantum state. If each configuration in the wave function is written as $|s_1,\ldots,s_N\rangle$ where s_i denote local quantum degrees of freedom such as the spin S_i^z on the ith lattice site and N is the total number of sites in the lattice, a MPS representation for the wave function $|\Psi\rangle$ is written as

$$|\Psi\rangle = \sum_{s_1,\ldots,s_N} \mathrm{Tr}\left[A^1_{s_1}\cdots A^N_{s_N}\right]|s_1,\ldots,s_N\rangle. \qquad (1)$$

In Eq. (1) the weight of each configuration is given by the trace of a product of $D\times D$ matrices A^i_{jk} The advantage of using a MPS representation is that it can provide an accurate representation of the ground state of a 1D quantum system with only moderate [5,6] values of D. Equation (1) can be used to represent a 2D system by simply numbering the lattice sites in two dimensions sequentially [as in Fig. 1(a)], but favorable scaling with the matrix size D is then lost because the MPS ansatz can only describe entanglement along the chain direction. Nevertheless, despite the exponential scaling of the number of states that must be kept (m) with the transverse lattice size, DMRG has been used to study 2D systems [7].

A recent innovation is the use of Monte Carlo sampling to evaluate expectation values of the Hamiltonian as well as other operators within MPS-type trial states [8–11]. By sampling the physical states of the system rather than contracting the matrices, the computational scaling in D can be reduced in some cases, particularly for systems with periodic boundaries [8,9]. Derivatives of the energy with respect to the matrix elements can also be calculated and then used to optimize [8,10] the matrix elements A^i_{jk}. The use of QMC sampling brings the computational advantage of trivial parallelization of Monte Carlo averages. While most applications have been to quantum spin models, this approach has successfully been used for more complicated quantum models such as the 1D Hubbard model where each site has four rather than two degrees of freedom [12].

Many variations of the MPS ansatz have been suggested to generalize it to 2D systems. The most natural extension to higher dimensions is to replace the matrices in Eq. (1) by tensors and the trace by a more general contraction over the tensor indices. A number of tensor-product state ansatzes have been proposed [13–18] (see Refs. [19] and [20] for reviews). One promising generalization of MPS are projected entangled pair states (PEPS) [18]. PEPS have been successfully applied to 2D frustrated spin models [21–23]. A variation (iPEPS) has also been proposed for evaluating thermodynamic (infinite lattice) quantities [24–26]. The main limitation in applying tensor-product ansatzes to numerical calculations is the poor computational scaling in the tensor size (typically proportional to D^{12} for PEPS [19]). A variety of other approaches use the same ansatz states as PEPS but different approximate algorithms to evaluate expectation values. Examples include the second renormalization of tensor networks (SRG) method [27,28] and the tensor-renormalization group (TRG) method [29,30]. Another generalization of MPS is the multiscale entanglement renormalization ansatz (MERA) [31,32]. MERA can be exactly contracted in polynomial time with somewhat worse scaling in D compared to PEPS algorithms (proportional to D^{16} for the algorithm proposed in Ref. [32]).

Applications to fermionic systems bring additional challenges to tensor network methods. In an occupation number representation the sign of each configuration necessarily depends on the ordering of the fermionic creation operators. While trivial in one dimension where the Jordan-Wigner transformation can be used to map fermionic operators to local spin operators, such a mapping is not usually possible in two dimensions. We note that this does not necessarily lead to long-range entanglement in the quantum state however. One of the key questions is whether it is possible to come up with an effectively local tensor network scheme for fermions and to what degree the difficulty of doing this depends on the model in

*r.t.clay@msstate.edu

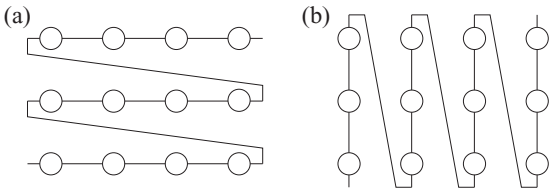

FIG. 1. Contraction patterns for (a) string S_A composed of A matrices and (b) string S_B of B matrices, illustrated for a 4×3 lattice.

question. Several approaches have nevertheless been proposed to treat fermionic systems by making the required tensor operations local. Examples include the modification of MERA by introducing fermionic swap gates [33,34] and fermionic versions of PEPS [35–38]. These modifications in general only modify the prefactor in the computational complexity scaling with D of the bosonic algorithms, so the principal disadvantage to using these methods for practical calculations remains the poor scaling of the bosonic algorithm.

An alternate approach to PEPS or MERA is to use a somewhat more restricted ansatz that can be more easily computationally evaluated. The promise is that one can trade some complexity of the representation by increasing the number of variational parameters. In this paper we will explore a generalization of one such approach, the string-bond states (SBS) ansatz, where several one-dimensional MPS strings of matrices are placed in different directions on the 2D lattice [9,10]. Other methods closely related to SBS are correlator product states [39] (CPS) and complete-graph tensor network states [40] (CGTN). The advantage of this class of methods is that the computational scaling in matrix size D remains small while potentially avoiding the exponential scaling in D with transverse size in DMRG calculations. The disadvantage is that the additional parameters lead to a more challenging optimization problem. We will show that in practice good results for 2D fermionic systems on significant lattice sizes (up to 12×12) can be reached within the SBS approximation.

The paper is organized as follows. Details of our SBS-QMC method are discussed in Sec. II. In Sec. III we show results for a 2D interacting spinless fermion system, followed by further discussion in Sec. IV.

II. METHOD

For a generic Hubbard-type model we decompose the Hamiltonian into two terms,

$$H = H_0 + H_1, \tag{2}$$

where diagonal H_0 and off-diagonal H_1 terms are given by

$$H_0 = U \sum_i n_{i\uparrow} n_{i\downarrow} + \sum_{\langle i,j\rangle} V_{ij} n_i n_j, \tag{3}$$

$$H_1 = -\sum_{\langle i,j\rangle\sigma} t_{ij} (c^\dagger_{j\sigma} c_{i\sigma} + c^\dagger_{i\sigma} c_{j\sigma}). \tag{4}$$

In Eqs. (3)–(4), $c^\dagger_{i\sigma}$ ($c_{i\sigma}$) create (annihilate) an electron of spin σ on site i, $n_{i\sigma} = c^\dagger_{i\sigma} c_{i\sigma}$, and $n_i = n_{i\uparrow} + n_{i\downarrow}$. We assume here that the nearest-neighbor sites in H_1 are those on a conventional square lattice, although as discussed later, it is possible to generalize this to other periodic lattices. U and V_{ij} are on-site and intersite Coulomb interactions. The weight of a configuration in the SBS approximation is represented in terms of overlaps defined on a set of operator strings $\{S\}$:

$$\langle C_n|\Psi\rangle = \prod_S \mathrm{Tr}\left[\prod_i S^i\right], \tag{5}$$

where $|C_n\rangle$ is a state in a local (e.g., occupation number) basis and the index n runs over all possible configurations. In Eq. (5) S^i are $D \times D$ real symmetric matrices. The assumption of symmetric matrices implies a reflection symmetry about the center of each string [8]. Many possible string patterns can be used for the SBS ansatz [9,10]. As shown in Fig. 1 we use a set of two strings $\{S_A, S_B\}$ to cover the lattice, each of which corresponds to the usual snake generalization conventionally used to adapt a MPS state to a 2D geometry. The string S_A (S_B) follows the hopping integrals aligned along x (y). The matrices for these two strings are labeled A and B. The SBS representation for the wave function $|\Psi\rangle$ is written as

$$|\Psi\rangle = \sum_n W(C_n)|C_n\rangle, \tag{6}$$

where $W(C_n) = \prod_S W_S(C_n)$. The weights $W_S(C_n)$ for the two strings are given by

$$W_A(C_n) = \mathrm{Tr}\prod_{i\in S_A}^{N} A^i = \mathrm{Tr}\prod_{i_x=1}^{L}\left(\prod_{i_y=1}^{M} A^{M(i_x-1)+i_y}\right), \tag{7}$$

$$W_B(C_n) = \mathrm{Tr}\prod_{i\in S_B}^{N} B^i = \mathrm{Tr}\prod_{i_y=1}^{M}\left(\prod_{i_x=1}^{L} B^{M(i_x-1)+i_y}\right), \tag{8}$$

where i_x and i_y correspond to the x and y coordinates of site $i = (i_x, i_y)$ for a $L \times M$ rectangular lattice with the total number of lattice sites N.

The variational Monte Carlo (MC) method we use to evaluate the energy and other correlation functions is based on the method of Ref. [8]. We have previously shown that this method can be generalized to 1D fermionic systems [12], where the weight of a configuration is given by a MPS, i.e., a single string. Configurations $|C_n\rangle$ are sampled according to the weight $W(C_n)^2$. MC updates consist of interchanges of electrons of a given spin between neighboring sites. Updates are attempted first along the path of string S_A and then along the direction of string S_B. In this manner, a system of left and right matrices can be used to efficiently perform the MC sampling [8]. We create a series of left matrices $L_A^{i_x,i_y} = A^i L_A^{i_x,i_y+1}$ and $L_B^{i_y,i_x} = B^i L_B^{i_y,i_x+1}$ for $i_x = 1,\ldots,L$ and $i_y = 1,\ldots,M$. Sequentially visiting the site $i = (i_x, i_y)$ in either the horizontal x (for S_A) or vertical y (for S_B) direction, we attempt to interchange electrons between that site and its nearest neighbor $j = (j_x, j_y)$ until we have arrived at site $N = (L, M)$. If an update is accepted (or rejected) according an acceptance probability $p(C_n \to C_{n'}) = \min[W^2(C_{n'})/W^2(C_n), 1]$, the right matrices $R_A^{i_x,i_y} = R_A^{i_x,i_y-1} A^i$ and $R_B^{i_y,i_x} = R_B^{i_y,i_x-1} B^i$ are advanced, respectively. Once the R matrices for a given string have been stored, measurements of the energy and

derivatives of the energy are implemented by traversing the string in the reverse direction [8].

The energy estimator for the configuration C_n is

$$E(C_n) = \sum_{C_{n'}} \frac{W(C_{n'})}{W(C_n)} \langle C_{n'}|H|C_n\rangle. \tag{9}$$

In Eq. (9), the diagonal part of the energy $\langle H_0\rangle$ can simply be measured as an average over the configurations visited. Interchanges of electrons give contributions to the off-diagonal terms $\langle H_1\rangle$. In calculating the matrix element in Eq. (9) a sign due to fermion exchange must be included.

Within the MPS representation the derivative of the energy with respect to the each of the matrix elements can easily be calculated. For the A matrices of S_A this derivative is

$$\frac{\partial E}{\partial A^k_{ij}} = 2\left\langle \frac{E(C_n) - \langle E(C_n)\rangle}{W_A(C_n)} \frac{\partial W_A(C_n)}{\partial A^k_{ij}} \right\rangle, \tag{10}$$

where the derivatives of each trace can be written as

$$\frac{\partial W_A(C_n)}{\partial A^k_{ij}} = \frac{1}{1+\delta_{ij}} \left[Q^A_{ij}(k) + Q^A_{ji}(k) \right], \tag{11}$$

using $Q^A(k) = \prod_{i\neq k} A^i$. An identical expression is used for derivatives of the energy with respect to the B matrices.

The matrix elements A^k_{ij} and B^k_{ij} for $k = 1,\ldots,N$ are first initialized to random numbers in the interval $[-\frac{1}{2},\frac{1}{2}]$. We normalize the matrices so that their Frobenius norm is unity, i.e., $\frac{1}{D}\mathrm{Tr}(AA^T) = 1$. MC measurements for the energy, derivatives, and other correlation functions are block averaged as usual. After each block, matrix elements are updated using a stochastic optimization scheme [8]. Each matrix element A^k_{ij} is modified by a random amount in the direction indicated by the derivative of the energy,

$$A^k_{ij} \to A^k_{ij} - \delta \cdot R \cdot \mathrm{sgn}\left(\frac{\partial E}{\partial A^k_{ij}}\right) \theta\left(\left|\frac{\partial E}{\partial A^k_{ij}}\right| - \alpha\right). \tag{12}$$

Here R is a random number in the interval $[0,1)$, $\mathrm{sgn}(x)$ is the signum function of a real number x, and $\theta(x)$ is the unit step function. The parameter δ sets the maximum change for a matrix element. The parameter α restricts changes to only the matrix elements that have the most significant effect on the energy, those with the largest magnitude derivatives, and helps to reduce unwanted stochastic noise as optimization proceeds. We found some improvement in the performance of the stochastic optimization with a suitable choice of α.

Several MC blocks each followed by the update in Eq. (12) are then combined into one *step* labeled by the index k of the optimization algorithm. At each successive k the parameters δ and α are decreased by a multiplicative factor Q. For the results here, we typically used $Q = 0.9$. δ and α were initially chosen as 0.5. Simultaneously the number of MC blocks per step, $G(k)$, and samples per block, $F(k)$, are increased linearly, We typically used $F(k) = 5000$–10000 and $G(k) = 250$–500. This procedure gives an annealing procedure that for a sufficiently large k should approach the global minimum energy. The MC sampling was parallelized using an embarrassingly parallel' algorithm. The results presented here used up to 192 processors.

III. RESULTS

A. Model

We consider spinless fermions interacting with a nearest-neighbor Coulomb repulsion. The Hamiltonian is given by

$$H = -t \sum_{\langle ij\rangle} (c^\dagger_i c_j + \mathrm{H.c.}) + V \sum_{ij} n_i n_j. \tag{13}$$

In Eq. (13), $c^\dagger_i$ creates a fermion on site i and $n_i = c^\dagger_i c_i$; sites i and j in $\langle ij\rangle$ are nearest-neighbor pairs on a 2D square ($M = L$) lattice of $N = L^2$ sites with periodic boundary conditions. All energies will be given in units of t. We consider the half-filled case with $N/2$ particles. For this density, the V interaction causes a checkerboard pattern charge-ordered (CO) insulating phase. In the 1D limit the model may be transformed via the Jordan-Wigner transformation to a spin-$\frac{1}{2}$ XXZ Heisenberg model and it can be shown exactly that the CO phase occurs when $V > V_c$ with [41] $V_c = 2$. In two dimensions V_c is not known exactly. Analytical work using a slave-boson approximation was done for a model with SU(N) fermions [42]. For the case of a 2D square lattice and taking $N = 2$ (corresponding to spin-$\frac{1}{2}$) the corresponding $V_c = 0.69$. This model was also previously studied using finite-temperature determinantal QMC [43] down to temperatures of order $T \sim 0.5$. These numerical results were also compared with the mean-field RPA predictions [43]. If one extrapolates the strong-coupling RPA result from reference [43] to $T = 0$, $V_c \approx 1/\sqrt{3} \approx 0.58$. The finite-temperature QMC results for V_c appear to be consistent with this limit if an almost-linear extrapolation in the T-V plane is assumed, but could not rule out the possibility that $V_c \to 0$ as $T \to 0$. As shown below, our present results are consistent with a nonzero V_c.

B. Method verification

In this section we show a number of benchmarks of the SBS-QMC method, which demonstrate that (i) the stochastic optimization technique detailed above performs successfully for a range of model parameters, including the challenging region close to the quantum phase transition in Eq. (13); (ii) the SBS approximation itself scales favorably with the matrix size D, with the error of the method decreasing as a power law in D; and (iii) the results of SBS-QMC compare favorably to other methods, specifically DMRG.

An order parameter for the CO phase at half filling is the charge structure factor $S(\boldsymbol{q})$ at $\boldsymbol{q} = (\pi,\pi)$. $S(\boldsymbol{q})$ is defined as

$$S(\boldsymbol{q}) = \frac{1}{N} \sum_{j,k} e^{i\boldsymbol{q}\cdot\boldsymbol{r}_{jk}} \left\langle \left(n_j - \frac{1}{2}\right)\left(n_k - \frac{1}{2}\right)\right\rangle, \tag{14}$$

where $\boldsymbol{r}_{jk}$ is the vector between lattice sites j and k. Figure 2 shows how the relative error in the ground-state energy, $\Delta E = |(E_{\mathrm{QMC}} - E_{\mathrm{exact}})/E_{\mathrm{exact}}|$, and similarly the relative error in the charge structure factor, $\Delta S(\pi,\pi)$, change as a function of algorithm steps k and matrix size D for a 4×4 lattice. The interaction strength $V = 0.45$ chosen here is close to the CO transition, which is expected to be the most computationally challenging parameter region of the model. Here and in our following results each value of D is a separate calculation, each starting with different random initial matrix elements.

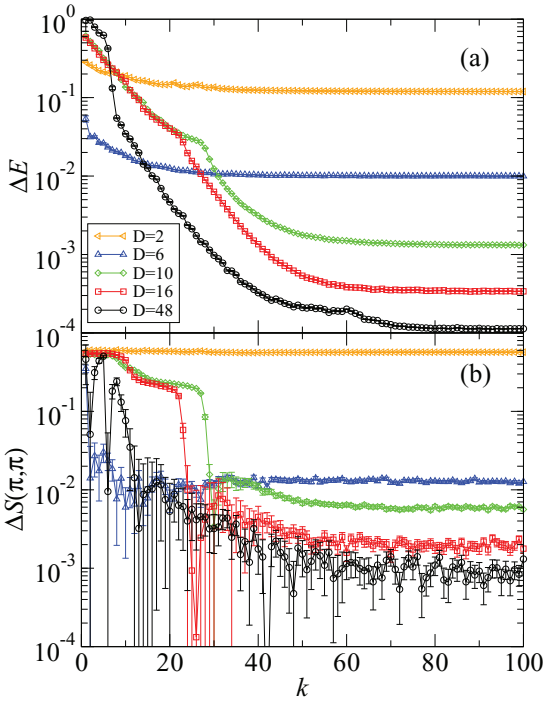

FIG. 2. (Color online) Relative error of the (a) ground-state energy and (b) charge structure factor at $S(\pi,\pi)$, as a function of the number of algorithm steps k (see text) and matrix size D for a 4×4 periodic lattice with eight particles and $V = 0.45$.

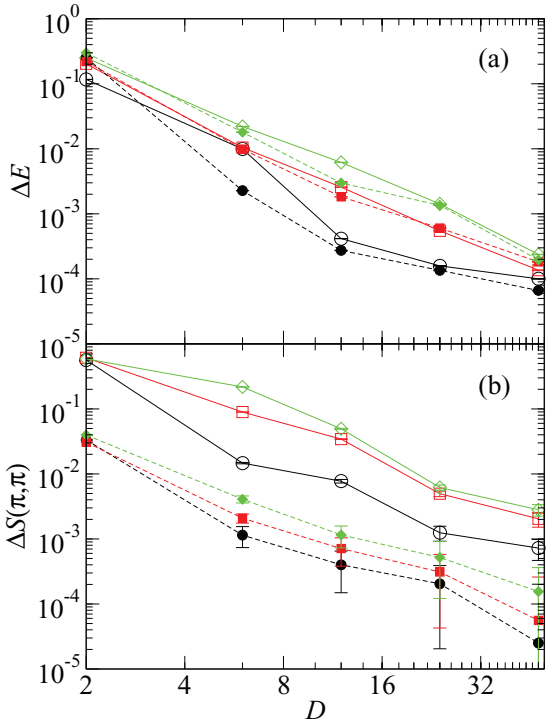

FIG. 3. (Color online) Relative error of the (a) ground-state energy and (b) of the charge structure factor as a function of matrix size D for $V = 0.45$ (open symbols) and $V = 4$ (filled symbols). Circles, squares, and diamonds are for 4×4, 6×4, and 8×4 lattices, respectively.

As can be seen in Fig. 2, due to the stochastic nature of the optimization technique, we find at certain k sudden decreases in the error, which correspond to the method finding its way out of a local minima. In subsequent results presented below, on of order 100 algorithm steps k were needed to converge the energy and other observables. We also found that it was useful to occasionally restart the optimization process to verify that the final results were adequately converged and not trapped in local minima.

Figure 3 summarizes the performance of SBS-QMC for 16, 24, and 32 site lattices as a function of matrix size D. Two different V are shown, $V = 0.45$ and $V = 4$. The slight scatter of the points rather than following a smooth decrease with D shows that some further small improvement to the optimization can be made. $V = 4$ is well within the CO phase of the model. As is expected for methods using a MPS ansatz, the method performs better in the gapped CO phase [19]. This is especially seen in the charge structure factor results in Fig. 3(b), which require significantly smaller D for comparable accuracy in the CO phase compared to the parameter region near the phase boundary.

At $V = 0$ the model is exactly soluble and in a metallic phase. Metallic phases present a large entanglement in real space and provide a challenging test for the method. Figure 4 shows the relative energy error for $V = 0$ and lattices from 16 to 64 sites. In all of the test cases we examined, we found that provided D is large enough, the accuracy of the SBS approximation decreases as a power law in D. From Figs. 3 and 4 we estimate that the error decreases as approximately D^{-2}.

Despite its shortcomings DMRG remains a powerful and widely used method for strongly correlated systems. Figure 5 compares SBS-QMC to DMRG calculations performed using the ALPS software package [44–46]. In the DMRG calculations we used cylindrical boundary conditions on $L \times M$ rectangular lattices, which were periodic in the transverse direction and open in the longitudinal direction [7]. With cylindrical boundaries, the number of DMRG states required (m) to reach a given accuracy scales exponentially with the length of the transverse lattice dimension M. In the results in Fig. 5 we used m of up to 2600 for the largest ($M = 10$) lattices; the maximum longitudinal lengths were $L = 24$ for $M = 4$, 6, and 8, and $L = 22$ for $M = 10$. The DMRG

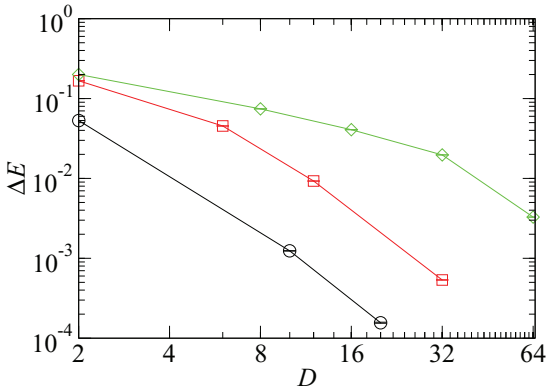

FIG. 4. (Color online) Relative error of the ground state energy as a function of matrix size D for $V = 0$. Circles, squares and diamonds are for 4×4, 6×6 and 8×8 lattices, respectively.

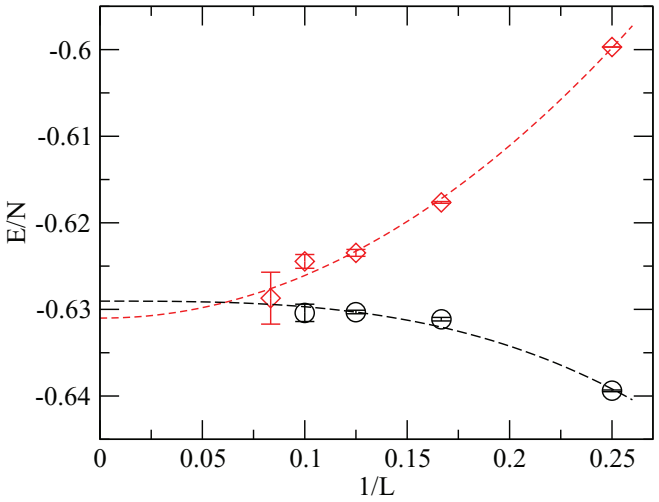

FIG. 5. (Color online) Comparison of SBS-QMC and DMRG finite-size scaling for $V = 0.45$. Diamonds (circles) are from SBS-QMC (DMRG). SBS-QMC simulations are on periodic $L \times L$ lattices, while points for DMRG are the extrapolated energies of infinite-length cylinders of width L. Lines are fits to the data (see text).

calculations were performed on a single CPU; somewhat larger transverse widths can be reached with parallel DMRG codes [7,47]. For each DMRG calculation we first performed a linear extrapolation in the DMRG truncation error ϵ followed by a linear extrapolation in $1/L$ over several lattices of the same width [7]. The energies of these infinite-length cylinders are plotted in Fig. 5 as a function of $1/M$. The SBS-QMC energies were similarly extrapolated to infinite D (see below). In general we found the extrapolation in D to be smooth and well behaved.

In Fig. 5 we show fits to the data using a quadratic function for the SBS-QMC data, and the form $a + bM^{-3}$ for the DMRG data [7]. Both methods give nearly the same energy extrapolated to the thermodynamic limit.

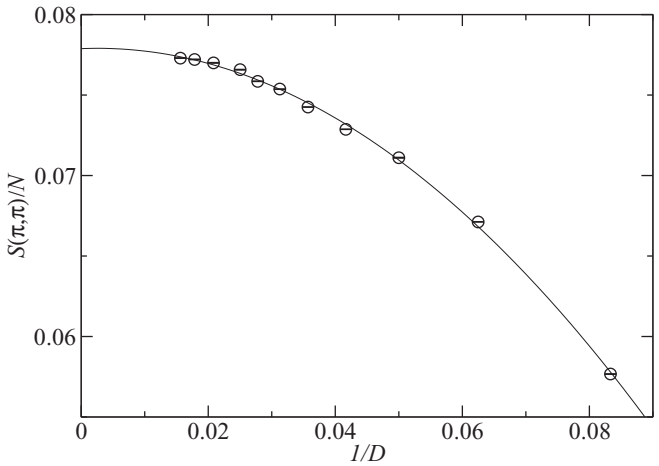

FIG. 6. The charge structure factor $S(\pi,\pi)$ as a function of matrix size D on a 12×12 lattice for $V = 0.8$. The line is a quadratic fit.

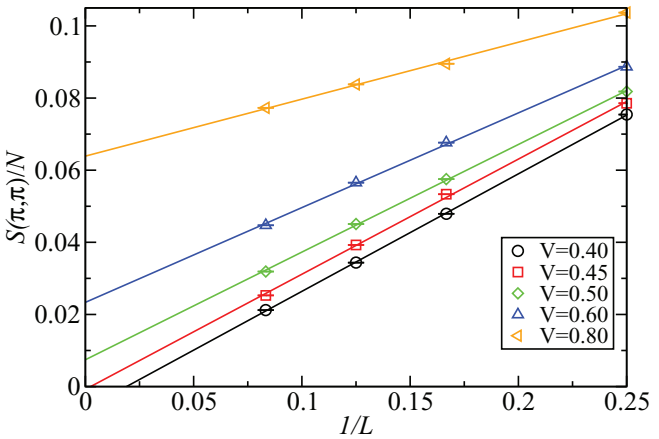

FIG. 7. (Color online) Finite-size scaling of the charge structure factor $S(\pi,\pi)$ versus $1/L$ for spinless fermions on square periodic lattices at half-filling. SBS-QMC simulations were performed for up to 12×12 systems; $S(\pi,\pi)$ for the 4×4 lattice was calculated exactly.

C. Phase diagram

In the CO phase of Eq. (13) $S(\pi,\pi)/N$ converges to a finite value in the thermodynamic limit. In order to precisely determine the V_c separating the metallic and CO phases of this model we calculated $S(\pi,\pi)$ over a range of V and system sizes. For each system we took D up to 64 and performed an extrapolation to $D \to \infty$. An example of this extrapolation in D is shown in Fig. 6 for the largest system studied, 12×12, with $V = 0.8$. Finally, Fig. 7 shows the finite-size scaling of $S(\pi,\pi)/N$. The results in Fig. 7 clearly show that a finite critical coupling V_c for the CO phase exists. By plotting the extrapolated $S(\pi,\pi)/N$ versus V, we estimate that $V_c = 0.45 \pm 0.02$

IV. DISCUSSION

In this paper we have presented numerical results using the SBS ansatz applied to a 2D fermionic model. In order to simulate a fermionic system we have used stochastic optimization to optimize both the sign and amplitude of a general SBS wave function. Because the computational scaling of the method is relatively small, this brute force optimization is successful for reasonably large fermionic systems, for example here up to $N = 144$. As the method is not restricted to unfrustrated lattices, we expect it will provide a useful way to study frustrated Hubbard-type models on lattice sizes out of reach of exact diagonalization.

In the SBS ansatz there are many possible choices for the form of the strings. For the form chosen here, two perpendicular snakes oriented in the transverse and longitudinal directions of the lattice, the scaling of the method is proportional to NMD^3 where M is the width of the lattice [8]. Our results indicate that with this string choice, the error in the SBS ansatz scales as approximately D^{-2}. An interesting question for future study is to determine the optimal string pattern—for example, the S_B string here can be taken not perpendicular to the S_A string, but oriented along the diagonal direction of the lattice. Because the QMC sampling involves particle exchanges along the string directions, sampling acceptance

rates and efficiency can also be influenced by the choice of the strings. Because this can improve the derivatives of the energy, such changes would also change the overall efficiency of the optimization.

Our comparison with DMRG provides further verification of the SBS-QMC method—both methods when extrapolated to the thermodynamic limit give comparable results. Comparing the two methods, DMRG benefits from being able to reach a large m and many years of algorithm refinements; it is clearly preferable for use on rectangular lattices of large aspect ratio provided M is not too large. One advantage of SBS-QMC is that square periodic lattices are in some cases easier to perform finite-size scaling on. Current DMRG calculations are limited to about $M = 12$, the same size reached in our SBS-QMC calculations. While available computer power will increase, the exponential scaling in the required m will make it difficult to push DMRG to larger lattices. Our results confirm that the SBS ansatz does not suffer from a similar limitation in scaling on M. Rather, the current limitation with calculations using the SBS ansatz is in how well the matrices can be optimized in practice. Further improvements to the algorithm presented here can certainly be made, particularly in the stochastic optimization of the matrix elements. For example, in applying SBS to 2D spin systems, it was noticed that the initial choice for the matrix elements could make a large difference in the convergence [10]. Here we have only used random starting matrices; using a mean-field or other approximate solution as the initial starting state could potentially improve the results significantly.

While we have presented data here for a spinless fermion model, we have tested the method for 2D Hubbard models including spin. Incorporating spin simply increases the number of states per site, and initial results show that this simply requires a larger D to obtain comparable accuracy in the energy and correlation functions.

ACKNOWLEDGMENTS

This work was supported by the US Department of Energy Grant No. DE-FG02-06ER46315. Part of the DMRG calculations were performed using resources of the National Energy Research Scientific Computing Center (NERSC), which is supported by the Office of Science of the US Department of Energy under Contract No. DE-AC02-05CH11231. We thank A. Sandvik for helpful discussions while preparing this manuscript. R.T.C. thanks the Condensed Matter Theory Visitor's Program at Boston University for hospitality while on sabbatical.

[1] H. Evertz, Adv. Phys. **52**, 1 (2003).
[2] S. R. White, Phys. Rev. Lett. **69**, 2863 (1992).
[3] S. R. White, Phys. Rev. B **48**, 10345 (1993).
[4] U. Schollwöck, Rev. Mod. Phys. **77**, 259 (2005).
[5] S. Rommer and S. Östlund, Phys. Rev. B **55**, 2164 (1997).
[6] U. Schollwöck, Ann. Phys. (N.Y.) **326**, 96 (2011).
[7] E. M. Stoudenmire and S. R. White, Ann. Rev. Condens. Matt. Phys. **3**, 111 (2012).
[8] A. W. Sandvik and G. Vidal, Phys. Rev. Lett. **99**, 220602 (2007).
[9] N. Schuch, M. M. Wolf, F. Verstraete, and J. I. Cirac, Phys. Rev. Lett. **100**, 040501 (2008).
[10] A. Sfondrini, J. Cerrillo, N. Schuch, and J. I. Cirac, Phys. Rev. B **81**, 214426 (2010).
[11] L. Wang, I. Pižorn, and F. Verstraete, Phys. Rev. B **83**, 134421 (2011).
[12] R. T. Clay, J.-P. Song, S. Dayal, and S. Mazumdar, J. Phys. Soc. Jpn. **81**, 074707 (2012).
[13] H. Niggemann, A. Klümper, and J. Zittartz, Z. Phys. B: Condens. Matter **104**, 103 (1997).
[14] H. Niggemann, A. Klümper, and J. Zittartz, Eur. Phys. J. B **13**, 15 (2000).
[15] K. Okunishi and T. Nishino, Prog. Theor. Phys. **103**, 541 (2000).
[16] N. Maeshima, Y. Hieida, Y. Akutsu, T. Nishino, and K. Okunishi, Phys. Rev. E **64**, 016705 (2001).
[17] Y. Nishio, N. Maeshima, A. Gendiar, and T. Nishino, arXiv:cond-mat/0401115.
[18] F. Verstraete and J. Cirac, arXiv:cond-mat/0407066.
[19] F. Verstraete, V. Murg, and J. Cirac, Adv. Phys. **57**, 143 (2008).
[20] R. Orús, arXiv:1306.2164v2.
[21] A. Isacsson and O. F. Syljuåsen, Phys. Rev. E **74**, 026701 (2006).
[22] B. Bauer, G. Vidal, and M. Troyer, J. Stat. Mech. (2009) P09006.
[23] V. Murg, F. Verstraete, and J. I. Cirac, Phys. Rev. B **79**, 195119 (2009).
[24] J. Jordan, R. Orús, G. Vidal, F. Verstraete, and J. I. Cirac, Phys. Rev. Lett. **101**, 250602 (2008).
[25] R. Orús and G. Vidal, Phys. Rev. B **80**, 094403 (2009).
[26] G. Vidal, Phys. Rev. Lett. **98**, 070201 (2007).
[27] Z. Y. Xie, H. C. Jiang, Q. N. Chen, Z. Y. Weng, and T. Xiang, Phys. Rev. Lett. **103**, 160601 (2009).
[28] H. H. Zhao, Z. Y. Xie, Q. N. Chen, Z. C. Wei, J. W. Cai, and T. Xiang, Phys. Rev. B **81**, 174411 (2010).
[29] M. Levin and C. P. Nave, Phys. Rev. Lett. **99**, 120601 (2007).
[30] L. Wang, Y.-J. Kao, and A. W. Sandvik, Phys. Rev. E **83**, 056703 (2011).
[31] G. Vidal, Phys. Rev. Lett. **99**, 220405 (2007).
[32] G. Evenbly and G. Vidal, Phys. Rev. Lett. **102**, 180406 (2009).
[33] P. Corboz and G. Vidal, Phys. Rev. B **80**, 165129 (2009).
[34] P. Corboz, G. Evenbly, F. Verstraete, and G. Vidal, Phys. Rev. A **81**, 010303 (2010).
[35] P. Corboz, R. Orús, B. Bauer, and G. Vidal, Phys. Rev. B **81**, 165104 (2010).
[36] P. Corboz, J. Jordan, and G. Vidal, Phys. Rev. B **82**, 245119 (2010).
[37] C. V. Kraus, N. Schuch, F. Verstraete, and J. I. Cirac, Phys. Rev. A **81**, 052338 (2010).
[38] I. Pižorn and F. Verstraete, Phys. Rev. B **81**, 245110 (2010).
[39] H. J. Changlani, J. M. Kinder, C. J. Umrigar, and G. K.-L. Chan, Phys. Rev. B **80**, 245116 (2009).
[40] K. H. Marti, B. Bauer, M. Reiher, M. Troyer, and F. Verstraete, New J. Phys. **12**, 103008 (2010).

[41] F. Mila and X. Zotos, Europhys. Lett. **24**, 133 (1993).
[42] R. H. McKenzie, J. Merino, J. B. Marston, and O. P. Sushkov, Phys. Rev. B **64**, 085109 (2001).
[43] J. E. Gubernatis, D. J. Scalapino, R. L. Sugar, and W. D. Toussaint, Phys. Rev. B **32**, 103 (1985).
[44] Algorithms and Libraries for Physics Simulations (ALPS), http://alps.comp-phys.org/
[45] A. Albuquerque *et al.*, J. Magn. Magn. Mater. **310**, 1187 (2007).
[46] B. Bauer *et al.*, J. Stat. Mech. (2011) P05001.
[47] E. M. Stoudenmire and S. R. White, Phys. Rev. B **87**, 155137 (2013).